Sustainable Food Technology

ROYAL SOCIETY OF CHEMISTRY

PAPER

View Article Online
View Journal

Cite this: DOI: 10.1039/d6fb00038j

Production of tagatose-rich syrup with ion-exchange resin purification

Nilofar Arabi, Seyedamirreza Babaei, Ji Qi, Shubhangi Arvelli, Shaghayegh Janbazialamdari and Jikai Zhao *

The production of rare sugar syrups, particularly tagatose-rich syrups, has attracted increasing interest due to their low glycemic index and potential applications in reduced-sugar food products. Although CaO-promoted alkaline isomerization of galactose offers an efficient route for tagatose production, residual inorganic ions remaining after neutralization hinder achievement of higher quality. In this study, ion-exchange purification of tagatose–galactose syrup produced *via* CaO-promoted isomerization was systematically optimized. Following isomerization, the reaction mixture was neutralized using either CO_2 or sulfuric acid and purified using combinations of strong-acid cation and strong-base anion exchange resins. The effects of neutralization route, resin type, resin dosage, and contact time on electrical conductivity, mineral removal, pH stability, and color were evaluated. CO_2-neutralized syrups exhibited lower initial ionic strength and superior deionization performance compared with sulfuric-acid-neutralized syrups. The optimal resin system reduced syrup conductivity by approximately 90% to ≤250 μS cm^{-1} (measured on diluted samples), indicating effective deionization performance. Empirical second-order regression models (R^2 > 0.87, R^2 > 0.92); trendline slopes (0.97–0.94) were developed to guide process optimization. The purified syrup was subsequently concentrated to 65 and 75 °Brix leading to low ash content (0.09–0.13%), reduced water activity (~0.7), acceptable color (90 IU), low HMF formation (4.2 mg kg^{-1}) and no detectable pathogens. This work provides bench-scale ion-exchange design guidelines for CaO-isomerized tagatose–galactose syrups, with mass-balance-confirmed sugar preservation and ionic removal data that can inform future column-scale process development.

Received 11th February 2026
Accepted 10th May 2026

DOI: 10.1039/d6fb00038j

rsc.li/susfoodtech

Sustainability spotlight

A bench-scale pathway for producing low-glycemic rare sugar syrups is demonstrated by integrating CaO-promoted galactose isomerization with CO_2 neutralization and ion-exchange purification. This approach reduces inorganic salt residues and improves deionization efficiency, resulting in syrups with enhanced purity and quality. The resulting tagatose-rich syrups show promising characteristics for use as alternative sweeteners in reduced-sugar food applications, while further validation against industrial and regulatory standards is required.

1. Introduction

D-Tagatose is a rare ketohexose naturally present in trace amounts in dairy products. With a caloric value of 1.5 kcal g^{-1}, a glycemic index of approximately 3, and sweetness equivalent to roughly 92% of sucrose, it has attracted substantial interest as a functional bulk sweetener for reduced-sugar and low-calorie food formulations.[1,2] Beyond its nutritional profile, D-tagatose exhibits prebiotic activity and has demonstrated beneficial effects on blood glucose regulation, dental health, and gut microbiota composition, positioning it as a multifunctional food ingredient rather than a simple sugar substitute.[3–5]

D-Tagatose is produced commercially by isomerization of D-galactose, which is obtained by hydrolysis of lactose from dairy sources such as whey permeate.[3] Both enzymatic and chemical isomerization routes have been developed. Enzymatic routes using L-arabinose isomerase offer high selectivity and mild conditions, but face challenges related to enzyme cost, thermal instability, and metal ion dependency that constrain industrial competitiveness.[6,7] Chemical isomerization using calcium hydroxide [$Ca(OH)_2$] remains one of the most efficient non-enzymatic routes, capable of achieving tagatose yields exceeding 70% under ambient conditions through the formation of a $Ca(OH)_2$-tagatose complex intermediate that drives the equilibrium toward the ketose product and suppresses sugar degradation.[8] For simplicity, this system is hereafter referred to as CaO-promoted isomerization, reflecting the practical use of calcium oxide, which hydrates *in situ* to generate $Ca(OH)_2$.

Carl and Melinda Helwig Department of Biological and Agricultural Engineering, Kansas State University, Manhattan, KS 66506, USA. E-mail: jikaizhao@ksu.edu

The foundational chemistry of this route was established in seminal patents by Beadle, Saunders, and Wajda (U.S. Patents 5002612 and 5078796), which described the isomerization of D-galactose to D-tagatose *via* a $Ca(OH)_2$-tagatose complex intermediate, followed by neutralization with an inorganic acid or CO_2 to release free tagatose and precipitate calcium salts.[9,10] Those patents explicitly identified a combination of filtration and ion-exchange resin treatment as the necessary downstream steps to remove the resulting inorganic salts and obtain a purifiable tagatose solution, and noted that CO_2, H_2SO_4, HCl, and H_3PO_4 are all suitable neutralizing agents. However, neither patent characterizes how the specific choice of neutralizing agent affects the ionic composition of the post-neutralization syrup, nor how those differences influence the performance of downstream ion-exchange purification. A more recent patent by Oroskar *et al.* (U.S. Patent 9150938) described a process using $CaO/Ca(OH)_2$ isomerization of galactose from deproteinized whey, followed by H_2SO_4 neutralization, filtration, and simulated moving bed (SMB) chromatographic separation to simultaneously recover pure tagatose and enriched glucose.[11] Notably, this patent explicitly avoids a dedicated ion-exchange deionization step by design: the inventors argued that H_2SO_4 neutralization generates $CaSO_4$ precipitates of sufficiently low solubility to be removed by simple filtration (0.45 μm), making a subsequent ion-exchange stage unnecessary. The patent further noted that when HCl is used instead, the resulting soluble $CaCl_2$ salts cannot be removed by filtration and instead require an expensive ion exchange stage to isolate. This reasoning highlights a critical process-design choice: the feasibility of bypassing ion exchange depends on the neutralizing agent selected and the solubility of the calcium salt it produces. When CO_2 is used for neutralization, which generates carbonate/bicarbonate species rather than sulfate and produces no easily filterable precipitate under mild conditions, the residual ionic load cannot be removed by filtration alone, and ion-exchange deionization becomes essential. Neither the Beadle patents nor the Oroskar *et al.* patent addresses this scenario, leaving unanswered how CO_2 neutralization governs feed ionic composition or what resin conditions are required to achieve low-ionic-strength syrups from such feeds.

Following neutralization, the post-isomerization syrup inevitably contains residual inorganic ions and dissolved salts, including calcium, magnesium, sodium, and anion species, which elevate electrical conductivity and may adversely affect product color, stability, and compliance with food-relevant quality benchmarks.[12,13] The specific ionic profile depends strongly on the neutralizing agent: CO_2 neutralization converts dissolved calcium to $CaCO_3$, leaving primarily carbonate and bicarbonate ions in solution, while H_2SO_4 neutralization generates $CaSO_4$ as the precipitate but leaves a fraction of sulfate ions dissolved due to their partial solubility, resulting in a higher and compositionally distinct ionic load entering downstream purification.[8] In our previous work, CaO-promoted galactose isomerization combined with both CO_2 and H_2SO_4 neutralization yielded clarified tagatose-rich syrups following filtration; however, the dissolved ionic content in both cases remained above conductivity levels targeted for high-quality syrup production, establishing the need for an additional ion-exchange purification step.[14]

Ion-exchange resins are well-established in industrial sugar processing for demineralization, decolorization, and polishing of glucose, fructose, and high-fructose corn syrup (HFCS) streams.[15,16] Sequential strong-acid cation and strong-base anion exchange is the standard configuration for achieving low-ionic-strength, food-compatible syrups, and their performance is strongly dependent on feed composition, resin selection, and operating conditions.[17,18] Ion-exchange polishing has also been applied in enzymatic tagatose production routes. For example, Wen *et al.* demonstrated that sequential cation–anion exchange beds achieved a desalination rate of 93.8% in an integrated bioprocess for tagatose production from lactose, yielding a syrup of 97.9% purity prior to crystallization.[19] In a related study, ion-exchange chromatography was also employed as the core purification step in a whole-cell biotransformation process for co-production of D-tagatose and D-allulose from whey powder.[20] These studies confirm that ion-exchange deionization is a practical purification strategy for tagatose-containing syrups. However, both are based on enzymatic routes in which the ionic composition of the feed entering ion exchange, dominated by metal cofactors, buffer salts, and fermentation-derived species, differs substantially from that generated by CaO-promoted chemical isomerization, where calcium-rich precipitates and neutralization-derived anion species dominate the feed. Performance benchmarks and resin selection criteria established for enzymatic systems therefore cannot be directly transferred to CaO-isomerized feeds.

Ion-exchange performance is sensitive to feed ionic strength, ion speciation, resin type, dosage, contact time, and regeneration effectiveness. Inadequate regeneration leads to ionic leakage, pH instability, and reduced exchange capacity, all of which compromise product quality and process consistency.[15] An additional consideration specific to galactose-containing syrups is the potential for anion-exchange resins to catalyze isomerization or epimerization of galactose under alkaline conditions, as recently demonstrated by Hashimoto *et al.*[21] This underscores the importance of careful resin selection and operating pH control in tagatose–galactose systems.

Despite the established role of ion exchange in sugar processing and its early identification as a necessary step in CaO-based tagatose production, no systematic study has examined how the choice of neutralization agent governs the ionic composition of the feed entering ion exchange and, in turn, determines deionization efficiency and final syrup quality. As discussed above, this is not a peripheral question: the Oroskar *et al.*[11] patent explicitly chose to avoid ion exchange by using H_2SO_4, which produces an easily filtered precipitate. The practical alternative, CO_2 neutralization, which is safer, generates no sulfate residues, and avoids introduction of exogenous anions, produces a fundamentally different ionic environment in which ion-exchange deionization cannot be bypassed. CO_2 and H_2SO_4 neutralization generate different post-neutralization anion distributions, different residual calcium speciation, and different overall ionic strengths, all of which directly affect resin

capacity utilization, conductivity reduction efficiency, and the operating conditions required to meet food-relevant quality benchmarks. Characterizing this coupling between neutralization chemistry and ion-exchange performance is therefore essential for establishing a rational process design basis for CaO-isomerized tagatose–galactose syrups.

Therefore, the objective of this study is to systematically evaluate how the upstream neutralization strategy governs downstream ion-exchange performance in CaO-promoted tagatose–galactose systems. By comparing CO_2 and H_2SO_4 neutralization routes across a range of resin combinations, dosages, and contact times, this work aims to identify the key variables controlling deionization efficiency, ionic removal, and syrup quality, and to develop empirical bench-scale operating guidelines that can inform future process development for tagatose–galactose syrup production.

2. Method and material

2.1. Preparation of tagatose–galactose feed syrup

D-(+)-Galactose (≥99%, Sigma-Aldrich, USA) was dissolved in deionized water to prepare a 0.5 M aqueous solution. Calcium oxide (CaO, analytical grade, Fisher Scientific, USA) was added at a 1 : 1 molar ratio (CaO/galactose) under continuous stirring at room temperature to initiate alkaline isomerization toward D-tagatose. Following isomerization, the reaction mixture was neutralized using either CO_2 or H_2SO_4 (98%, Fisher Scientific, USA) to remove excess calcium species.

For CO_2 neutralization, the reaction mixture containing the Ca-tagatose gel complex was transferred to a carbonation device (SodaStream International Ltd, United Kingdom), and CO_2 was bubbled through the solution at room temperature for 3–5 min. This step facilitated the conversion of dissolved calcium species to calcium carbonate ($CaCO_3$), as indicated by visible precipitation and stabilization of pH. For acid neutralization, concentrated H_2SO_4 was slowly added dropwise under stirring to promote precipitation of calcium sulfate. The formation of precipitates and stabilization of pH suggested effective neutralization, although complete precipitation was not independently verified. Following neutralization, all suspensions were allowed to settle for 30 min and subsequently filtered under a membrane-based vacuum filtration (Corning, Fisher Scientific, USA) to remove $CaCO_3$ or $CaSO_4$ precipitates. The clarified syrup (≈7 °Brix, density 1.028 g mL^{-1}, conductivity ≈ 2.6 mS cm^{-1}, pH ≈ 7) was stored at 4 °C prior to deionization experiments.

2.2. Ion-exchange resins and regeneration

Four commercial ion-exchange resins (DIAION®, Mitsubishi Chemical, Japan) were evaluated: two strong-acid cation exchangers, PK212 and SK1B (capacity ≈ 1.5 meq mL^{-1}), and two strong-base anion exchangers, PA312 and HPA25L (capacity ≈ 1.2 meq mL^{-1}). Prior to use, all resins were prewashed with deionized water, sieved to remove fines (<100 μm), and regenerated. Cation exchangers were regenerated in 0.5 M HCl and anion exchangers in 0.3 M NaOH by soaking 2 g resin portions in regenerant for 30 min at room temperature. Resins were rinsed repeatedly with deionized water until the effluent conductivity was ≤ 200 μS cm^{-1} and the pH stabilized between 6.5 and 7.0. Successful regeneration was verified by stabilization of rinse conductivity, indicating removal of residual regenerant and attainment of the desired ionic form.

2.3. Batch deionization experiments

Batch deionization experiments were conducted using 25 mL aliquots of CO_2- or H_2SO_4-neutralized syrup. Batch operation was selected to enable rapid screening of resin combinations and operating conditions prior to column-scale implementation. Each run consisted of sequential cation and anion exchange treatments using the resin combinations listed in Table 1. For each stage, 2 g of resin were added to the syrup and stirred at 500 rpm and 25 ± 1 °C for 20 min. Resins were removed by vacuum filtration, and conductivity and pH of the filtrates were measured immediately. The cation-treated syrups were transferred to fresh vessels containing regenerated anion resins for a second 20-min treatment under identical conditions. Sugar composition (galactose, tagatose, by-products) was verified by HPLC, and elemental analysis (Ca, Mg, Na, S, Fe, Cu, Mn, As, Pb, Cd, Hg) was quantified by ICP-OES. Apparent dilution factors were calculated as the ratio of the initial sugar concentration (before deionization) to the corresponding concentration after deionization. All experiments were performed in duplicate.

2.4. Evaporation and final syrup quality evaluation

Deionized syrup obtained under optimized ion-exchange conditions (7–8 °Brix, conductivity ≈ 250 μS cm^{-1}) was concentrated by controlled vacuum evaporation. Evaporation was carried out using a rotary vacuum evaporator (Büchi R-100, Switzerland) operated at 50 °C and −0.08 MPa until target soluble-solids contents of 65 and 75 °Brix were reached. Duplicate batches ($n = 2$) were prepared, and samples were collected at two concentration stages, after reaching 65 °Brix and after reaching 75 °Brix, yielding four evaporated syrup samples in total.

Following evaporation, syrup samples were stored in sealed containers at 4 °C prior to analysis. Physicochemical and compositional analyses were performed immediately after concentration. These analyses included color (A_{420} and ICUMSA), water activity, ash content, electrical conductivity, pH, sugar composition (HPLC), and mineral composition (ICP-OES). Microbiological quality was evaluated by total aerobic mesophilic count (TAMC), total yeast and mold count (TYMC), and detection of foodborne pathogens (*Escherichia coli*, *Salmonella* spp., and *Staphylococcus aureus*) in accordance with the FDA Bacteriological Analytical Manual (BAM). Microbiological analyses were conducted after approximately two weeks of refrigerated storage to assess microbial stability of the concentrated syrups under realistic handling and storage conditions.

2.5. Analytical methods

Electrical conductivity and pH were measured at 25 ± 0.5 °C using a calibrated benchtop meter (Sper Scientific, USA). To reduce viscosity-related artifacts associated with high-Brix sugar syrups, conductivity measurements were performed on ten-fold diluted samples prepared with deionized water. These measurements represent method-defined values for comparative purposes and do not correspond to the absolute conductivity of the native concentrated syrups. Soluble-solids content (°Brix) was determined using a digital refractometer (AgTec Portable Refractometer, USA). Water activity (a_w) was measured at 25 °C after a 10 min equilibration period using a water-activity meter (AquaLab 4TE, USA). Sugar compositions (tagatose, galactose, and minor sugars) were quantified by high-performance liquid chromatography (HPLC) using an Agilent 1200 HPLC system equipped with a refractive index (RI) detector and a Rezex RPM-monosaccharide column (Phenomenex, USA). Deionized water was used as the mobile phase at a flow rate of 0.6 mL min^{-1}, and the column temperature was maintained at 80 °C. 5-Hydroxymethylfurfural (HMF) was quantified using an Agilent Technologies 1260 Infinity HPLC system equipped with a UV detector and a Bio-Rad Aminex HPX-87H ion-exclusion column (300 × 7.8 mm). The column temperature was maintained at 65 °C, and 5 mM H_2SO_4 was used as the mobile phase at a flow rate of 0.6 mL min^{-1}. Quantification of tagatose and galactose was performed using external calibration with analytical standards over an appropriate concentration range. Calibration curves exhibited linear responses (R^2 > 0.99), and concentrations were determined based on peak area. Analytical accuracy was further evaluated by calculating mass-based sugar recovery across the deionization step using measured pre- and post-treatment concentrations and corresponding liquid volumes (see Section 3.5); recovery values of 90–113% across all runs confirmed the absence of systematic analytical bias or selective sugar loss during processing. All measurements were conducted in duplicate, and variability between replicates was within acceptable limits. HMF concentrations were quantified using external calibration with standard solutions. Calibration curves exhibited linear detector response, and concentrations were determined based on peak area. Elemental composition (Ca, Mg, Na, S, Fe, Cu, Mn, As, Pb, Cd, Hg) of initial, deionized, and evaporated syrups was determined by ICP-OES (Agilent 5800, USA) following dilution in 2% HNO_3 with external calibration. Ash content was analyzed according to AOAC 923.03 by drying 2–3 g of syrup in porcelain crucibles and ashing at 550 °C for 6 h in a muffle furnace (Thermo Scientific, USA) until constant mass. Color at 420 nm (A_{420}) was measured using a UV-vis spectrophotometer (Thermo Scientific BioMate 3, USA) with 1 cm quartz cuvettes. For high-solids syrups (65–75 °Bx), absorbance was measured on 10× diluted samples, and ICUMSA color values were calculated according to ICUMSA Method GS2/3-9 (2005).[22]

$$\mathrm{ICUMSA(IU)} = \frac{1000 \times A_{420}}{b \times c} \quad (1)$$

where A_{420} is the color absorbency at 420 nm, b is the optical path length (cm) and c is the concentration of the diluted sample (g mL^{-1}). All analytical measurements were performed in duplicate, and results are reported as mean values.

3. Results and discussion

3.1. Galactose isomerization performance

Galactose conversion and tagatose selectivity were quantified for each of the eight experimental runs listed in Table 1 following CaO-promoted isomerization and subsequent neutralization using CO_2 or H_2SO_4 (Fig. 1). Feed syrup preparation followed the protocol established in our previous work, and the resulting conversion and selectivity values were consistent with those previously reported for alkaline CaO-promoted isomerization systems.[14] Galactose conversion values ranged from approximately 83% for CO_2-neutralized syrups (runs 1–4) to approximately 90% for H_2SO_4-neutralized syrups (runs 5–8), indicating that high conversion was achieved under both neutralization routes. Similarly, tagatose selectivity values were approximately 53% for CO_2-neutralized feeds and 71% for H_2SO_4-neutralized feeds, remaining within the expected range for base-catalyzed isomerization. Although modest differences in selectivity were observed between the two neutralization routes, both approaches yielded chemically stable and compositionally consistent feed syrups suitable for subsequent deionization and purification studies. The observed difference in selectivity between CO_2- and H_2SO_4-neutralized systems is attributed to differences in the neutralization pathway rather than the formation of chemically distinct products. In both cases, the final product is D-tagatose. However, sulfuric acid neutralization leads to a rapid quench of the alkaline reaction environment, which can suppress side reactions and result in higher apparent selectivity. In contrast, CO_2 neutralization proceeds through carbonate equilibria and a more gradual pH adjustment, which may allow limited side reactions to occur. While the H_2SO_4-neutralized system exhibits

Table 1 Operating conditions for the screening of ion-exchange resin combinations under CO_2- and H_2SO_4-neutralized syrup conditions. All experiments were conducted using a galactose concentration of 0.5 M, a CaO/galactose molar ratio of 1 : 1, syrup volume of 25 mL, resin mass of 2 g for each resin, contact time of 20 + 20 min, stirring speed of 500 rpm, temperature of 25 °C, and vacuum filtration for solid removal[a]

Run no.	Neutralization acid	Cation resin type	Anion resin type
1	CO_2	Cation A	Anion A
2	CO_2	Cation A	Anion B
3	CO_2	Cation B	Anion A
4	CO_2	Cation B	Anion B
5	H_2SO_4	Cation A	Anion A
6	H_2SO_4	Cation A	Anion B
7	H_2SO_4	Cation B	Anion A
8	H_2SO_4	Cation B	Anion B

[a] Cation A = DIAION PK212, cation B = DIAION SK1B, anion A = DIAION PA312, anion B = DIAION HPA25L.

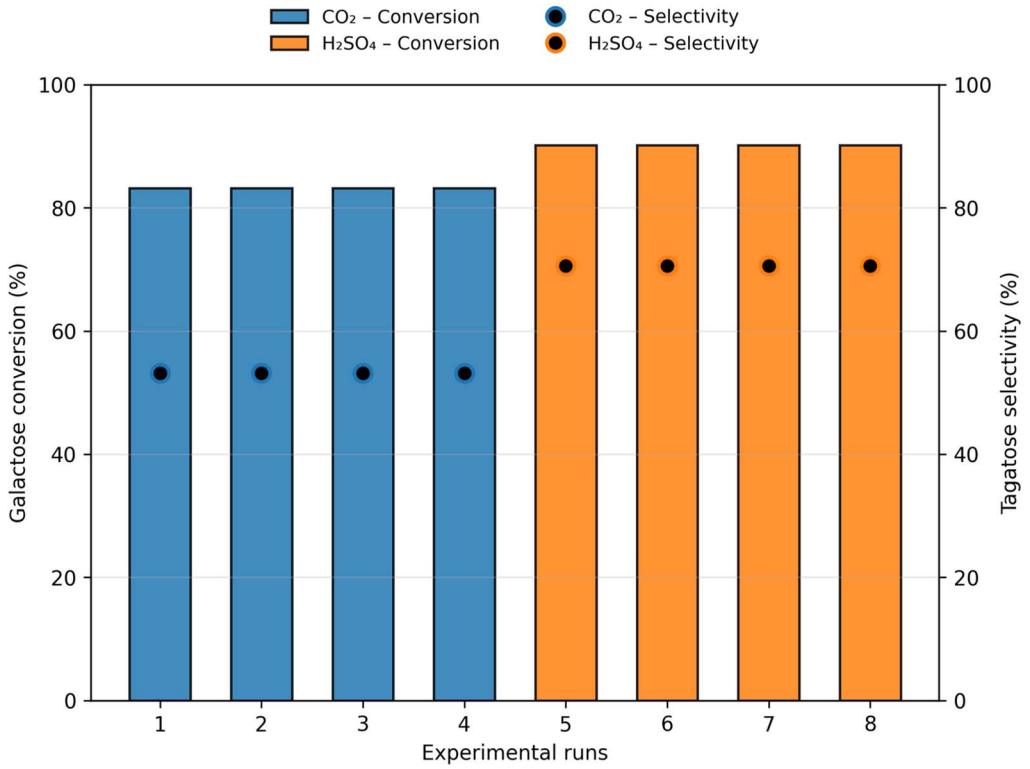

Fig. 1 Galactose conversion (bars) and tagatose selectivity (circles) following CaO-promoted isomerization for the eight experimental runs. Values represent the average of duplicate analytical measurements for each feed syrup; identical values across runs reflect the use of the same feed syrup for multiple experimental runs.

higher selectivity at the reaction stage, it also introduces higher inorganic content, which can increase the ionic load and complicate downstream purification. In contrast, CO_2 neutralization provides a more favorable balance between reaction performance and subsequent deionization.

3.2. Effect of neutralization route on ionic conductivity

The conductivity of the tagatose–galactose syrup prior to deionization varied markedly with the neutralization route (Fig. 2). Syrups neutralized with CO_2 exhibited an initial conductivity of approximately 2.6 mS cm^{-1}, whereas those neutralized with H_2SO_4 showed a higher value of 3.16 mS cm^{-1}. This difference arises from the distinct ionic species introduced during neutralization: CO_2 neutralization forms soluble bicarbonate and carbonate ions (HCO_3^-, CO_3^{2-}), whereas H_2SO_4 generates sulfate ions (SO_4^{2-}) that tend to remain dissociated even after partial Ca^{2+} precipitation.[23] Following ion-exchange treatment, the conductivity of all CO_2-neutralized syrups decreased substantially, reaching 262–902 μS cm^{-1}, while H_2SO_4-neutralized syrups showed more variable reductions (442–1728 μS cm^{-1}). The greater ionic strength in the H_2SO_4 system likely resulted from incomplete removal of divalent sulfate salts and slower ion diffusion within the resin pores due to higher ionic density. These findings confirm that the composition of neutralizing agents significantly influences the downstream deionization load and therefore must be optimized prior to large-scale operation. The greater difficulty in removing sulfate from H_2SO_4-neutralized feeds is consistent with the higher hydration energy of SO_4^{2-} relative to HCO_3^-/CO_3^{2-}, which results in stronger competition for resin exchange sites and reduced ion mobility within the resin pores under the batch contact conditions used here; however, direct confirmation of this mechanism would require speciation-resolved analytical measurements beyond the scope of the present study.

3.3. Screening of cation–anion resin combinations & color absorbency

The performance of the four cation–anion resin pairs is summarized in Fig. 2, considering both conductivity reduction and color absorbency (A_{420}) before and after ion-exchange treatment. For the CO_2-neutralized syrup (runs 1–4), the untreated feed exhibited conductivities of approximately 2600 μS cm^{-1} with relatively low initial color absorbency ($A_{420} \approx$ 0.045–0.050). Following resin treatment, substantial reductions in conductivity were observed, particularly for the cation A–anion A combination (run 1), which reduced conductivity to ≈ 262 μS cm^{-1} and simultaneously lowered absorbency to ≈ 0.020. The cation A–anion B system (run 2) showed a similar trend, reducing conductivity to ≈ 420 μS cm^{-1} with a final absorbency of ≈ 0.025. In contrast, systems containing cation B (runs 3–4) retained higher residual conductivities (≈675–902 μS cm^{-1}) and correspondingly higher absorbency values (≈0.030–0.035), indicating less effective removal of both ionic and colored species.

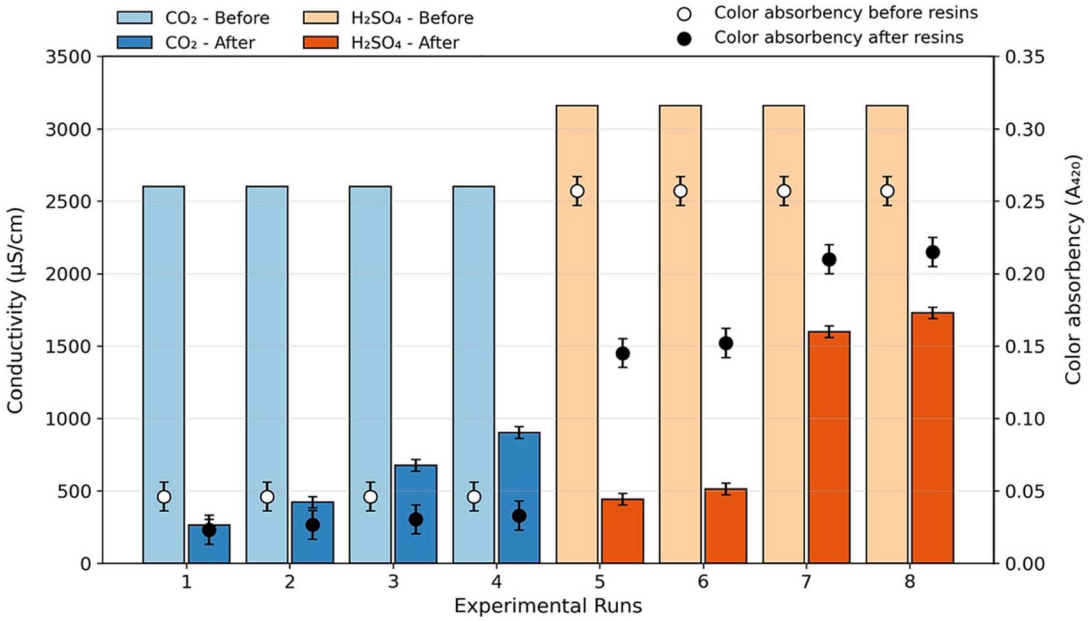

Fig. 2 Effect of resin treatment on syrup conductivity for CO_2- and H_2SO_4-neutralized tagatose-galactose syrups on conductivity and color absorbency (color-coded by neutralization type). Bars represent mean values of duplicate measurements, and error bars indicate standard deviations. Initial conductivity values showed no variability across runs and are therefore presented without error bars.

For the H_2SO_4-neutralized syrup (runs 5–8), the untreated samples exhibited markedly higher conductivities (≈3160 µS cm^{-1}) and significantly darker color (A_{420} ≈ 0.26), reflecting greater color formation during acid neutralization. After ion exchange, runs 5 and 6 (cation A-based systems) reduced conductivity to ≈ 442 and 512 µS cm^{-1}, respectively, with absorbency decreasing to ≈ 0.145–0.155. In contrast, systems containing cation B (runs 7–8) showed limited conductivity reduction (≈1598–1728 µS cm^{-1}) and retained higher absorbency (≈0.21–0.22). The difference in syrup color between H_2SO_4 and CO_2-neutralized samples is illustrated in Fig. S1. Across both neutralization methods, lower final conductivity generally corresponded to lower A_{420} values, indicating that effective ion exchange also promoted partial decolorization. However, the relationship was not strictly linear, suggesting that while removal of inorganic ions contributes to color reduction, additional non-ionic chromophoric compounds remain.

3.4. Deionization performance and elemental composition

ICP-OES for the eight experimental runs provided insights into elemental changes during deionization, and the numerical trends broadly followed the conductivity trends observed for each resin-neutralization combination. The untreated CO_2-neutralized syrup (initial sample for runs 1–4) contained high Ca (813.7 ppm) and moderate Mg (38.2 ppm), consistent with residual calcium originating from the CaO-based isomerization system (Table 2). Small quantities of sodium (≈2.1 ppm) were also detected, whereas trace metals such as Fe, Cu, Mn, Pb, As, and Cd were either absent or present only at sub-ppm levels. The presence of these trace elements is attributed to minor impurities in reagents (*e.g.*, CaO and neutralizing agents), residual ions in deionized water, and potential contributions from laboratory equipment or resin materials. The relatively consistent Mg concentration observed in the initial syrup suggests that it primarily originates from the starting materials rather than being introduced from materials used in the process.

After ion-exchange treatment, all four CO_2-neutralized runs showed substantial decreases in divalent elements, consistent with effective cation removal (Table 2). Calcium levels fell to 17–116 ppm depending on the resin pair, corresponding to removal efficiencies of approximately 86–98%. The lowest residual Ca (≈17–27 ppm) occurred in runs 1–3, which also achieved the lowest conductivities (262–675 µS cm^{-1}) (Table 2). Magnesium values similarly decreased from 38.2 ppm to 0.39–11 ppm, demonstrating effective Mg removal across all CO_2-neutralized runs. Sodium increased moderately after treatment (Na 12–29 ppm), which may be associated with resin regeneration chemistry and ion exchange processes. Trace metals remained minimal, with Cu, Mn, As, Pb, and Cd consistently below 0.05 ppm except for Hg (0.09 ppm) and Fe in the initial sample (0.40 ppm). The sulfuric acid-neutralized syrup (initial sample for runs 5–8) displayed a different elemental profile, with lower Ca (620 ppm), higher Mg (≈40 ppm), and elevated sulfur (≈1200 ppm), consistent with the use of sulfuric acid during neutralization (Table 2).

After resin treatment, calcium concentrations decreased only to 57–215 ppm, and magnesium to 4.3–7.2 ppm, indicating less efficient removal of divalent elements compared with the CO_2-neutralized system (Table 2). Sodium increased after treatment (Na 15–52 ppm), again reflecting interactions associated with resin operation. Elevated sulfur concentrations persisted in all

Table 2 Elemental composition of syrups before and after resin treatment (ICP-OES)[a]

	EC (μS cm^{-1})	Ca (ppm)	Mg (ppm)	Na (ppm)	S (ppm)	Fe (ppm)	Cu (ppm)	Mn (ppm)	As (ppm)	Pb (ppm)	Cd (ppm)	Hg (ppm)
Initial syrup for 1–4	2600	813.71	38.22	2.09	N.D.	0.40	N.D.	0.00	N.D.	N.D.	0.00	0.09
Run 1	262	16.83	0.39	12.01	N.D.	N.D.	0.01	0.01	N.D.	N.D.	0.00	0.01
Run 2	420	19.00	1.56	15.6	N.D.	N.D.	0.00	0.01	0.01	N.D.	0.00	0.01
Run 3	675	27.20	2.50	21.00	N.D.	N.D.	0.00	0.03	0.01	N.D.	0.00	0.01
Run 4	902	116.40	11.30	28.64	N.D.	N.D.	0.00	0.00	0.01	N.D.	0.00	0.00
Initial syrup for 5–8	3160	620	40.01	2.32	1200	0.40	N.D.	0.00	N.D.	N.D.	0.00	0.07
Run 5	442	57.12	4.26	15.57	350.58	0.01	0.03	0.20	0.01	N.D.	0.00	0.01
Run 6	512	65.30	4.83	22.07	520.02	N.D.	0.00	0.03	N.D.	N.D.	0.00	0.03
Run 7	1598	214.81	7.18	38.13	654.03	0.12	0.01	0.18	N.D.	N.D.	0.00	0.01
Run 8	1728	82.17	6.01	52.03	884.61	0.30	0.01	0.04	N.D.	0.00	0.00	0.01

[a] N.D. = not detected. EC = electrical conductivity.

H_2SO_4-neutralized runs (350–885 ppm), indicating the persistence of sulfur in the system following neutralization and treatment. These results are consistent with the higher post-treatment conductivity observed for acid-neutralized syrups and the greater difficulty in achieving low-ionic-strength conditions. As with the CO_2 system, trace metals (Pb, As, Cd, Hg) remained at very low levels, confirming that the process does not introduce hazardous elemental contaminants.

To provide a rigorous basis for assessing ionic removal independently of dilution effects, mass-based removal efficiencies were calculated for Ca, Mg, Na, and S by multiplying measured ICP-OES concentrations by the corresponding liquid volumes. The initial syrup volume was 25 mL for all runs; post-deionization volumes were calculated from the average dilution factor of galactose and tagatose (Section 3.5), ranging from 28.7 to 45.9 mL. The resulting ion mass balances are summarized in Table 3.

For CO_2-neutralized feeds (runs 1–4), Ca mass-based removal efficiencies ranged from 83.6% (run 4) to 97.0% (run 1). Mg removal ranged from 77.4% to 99.3%. Na mass increased after treatment in all CO_2 runs, consistent with Na^+ leaching from the NaOH-regenerated anion resin, confirming that conductivity reductions reflect cation removal rather than dilution artefacts. Sulfur was not detected in CO_2-neutralized feeds or effluents, consistent with the absence of sulfate in this neutralization pathway.

For H_2SO_4-neutralized feeds (runs 5–8), Ca mass-based removal ranged from 38.4% (run 7) to 83.8% (run 5), substantially lower than the CO_2 system due to the competing ionic load of residual dissolved sulfate. Sulfur mass removal ranged from 3.1% (run 7) to 48.5% (run 5), demonstrating that batch anion exchange can only partially reduce the sulfate load from H_2SO_4 neutralization. The low Ca and S removals in run 7 (38.4% and 3.1%, respectively) directly explain its highest residual conductivity (1598 μS cm^{-1}). The apparent negative S removal in run 8 falls within measurement uncertainty of duplicate ICP-OES determinations and is not interpreted as a net increase.

3.5. Sugar composition after deionization

To assess whether ion-exchange deionization selectively removed or transformed either sugar, absolute masses of galactose and tagatose were calculated before and after resin treatment by multiplying HPLC-measured concentrations (mM) by the corresponding liquid volumes (mL), yielding quantities in mmol. The initial volume was 25 mL for all runs; post-deionization volumes were estimated from the average dilution factor of galactose and tagatose, ranging from 28.7 to 45.9 mL (Table 4).

Galactose mass recovery across all eight runs ranged from 95.6% to 113.1%, and tagatose recovery from 89.6% to 104.8% (Table 4). Deviations from 100% are attributable to the combined measurement uncertainty of duplicate HPLC determinations and the volume estimation method. No systematic loss of either sugar was observed, and galactose and tagatose recoveries were statistically indistinguishable within each run. These results confirm that ion-exchange treatment does not selectively remove, degrade, or chemically transform either monosaccharide.

Table 3 Mass-based ion removal across ion-exchange runs. V_initial = 25 mL[a]

	Neutralization acid	V_fin (mL)	Ca IN (mg)	Ca OUT (mg)	Ca rem. (%)	S IN (mg)	S OUT (mg)	S rem. (%)
1	CO_2	35.7	0.0203	0.0006	97.0	N.D.	N.D.	N/A
2	CO_2	33.4	0.0203	0.0006	96.9	N.D.	N.D.	N/A
3	CO_2	34.7	0.0203	0.0009	95.4	N.D.	N.D.	N/A
4	CO_2	28.7	0.0203	0.0033	83.6	N.D.	N.D.	N/A
5	H_2SO_4	44.0	0.0155	0.0025	83.8	0.0300	0.0154	48.5
6	H_2SO_4	45.9	0.0155	0.0030	80.7	0.0300	0.0239	20.4
7	H_2SO_4	44.4	0.0155	0.0095	38.4	0.0300	0.0290	3.1
8	H_2SO_4	35.9	0.0155	0.0030	81.0	0.0300	0.0317	−5.7

[a] N.D. = not detected.

Table 4 Sugar mass balance. V_initial = 25 mL. Mass = concentration (mM) × volume (mL)/1000

Run	Neutralization acid	Galactose IN (mmol)	Galactose OUT (mmol)	Gal. rec. (%)	Tagatose IN (mmol)	Tagatose OUT (mmol)	Tag. rec. (%)
1	CO_2	2.425	2.539	104.7%	6.387	6.115	95.7%
2	CO_2	2.425	2.491	102.7%	6.387	6.221	97.4%
3	CO_2	2.425	2.743	113.1%	6.387	5.721	89.6%
4	CO_2	2.425	2.319	95.6%	6.387	6.702	104.8%
5	H_2SO_4	1.413	1.433	101.4%	9.186	9.067	98.6%
6	H_2SO_4	1.413	1.434	101.5%	9.186	9.059	98.6%
7	H_2SO_4	1.413	1.378	97.5%	9.186	9.413	102.5%
8	H_2SO_4	1.413	1.457	103.1%	9.186	8.930	97.2%

The apparent decrease in sugar concentration after deionization (reflected in dilution factors of 1.1–1.9, Fig. 3) is therefore attributable entirely to an increase in effective liquid volume resulting from water retained in the resin matrix and pore-space displacement during batch contact.[24] These phenomena are well-established in ion-exchange processing of carbohydrate syrups and do not represent sugar loss.[25,26] The downstream evaporation step (Section 2.4) reverses this dilution by concentrating the deionized liquor to the target °Brix.

3.6. Modelling and optimization of resin dosage

To quantitatively assess the influence of resin dosage and contact time on syrup deionization performance, empirical regression models were developed based on data from twelve

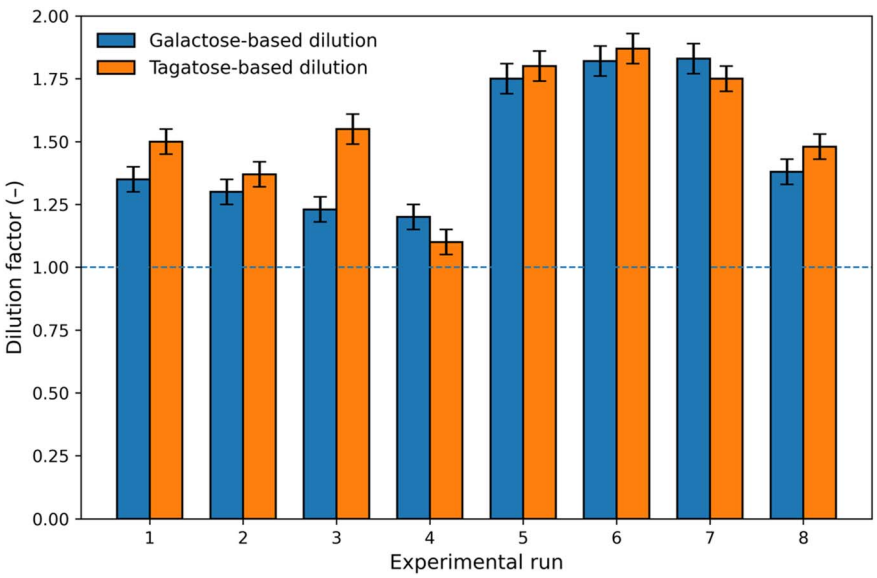

Fig. 3 Apparent dilution factors calculated independently from galactose and tagatose concentrations measured by HPLC before and after ion-exchange deionization for experimental runs 1–8. Error bars represent the standard deviation of duplicate measurements ($n = 2$). The dashed line at a dilution factor of 1 indicates the hypothetical case of no dilution.

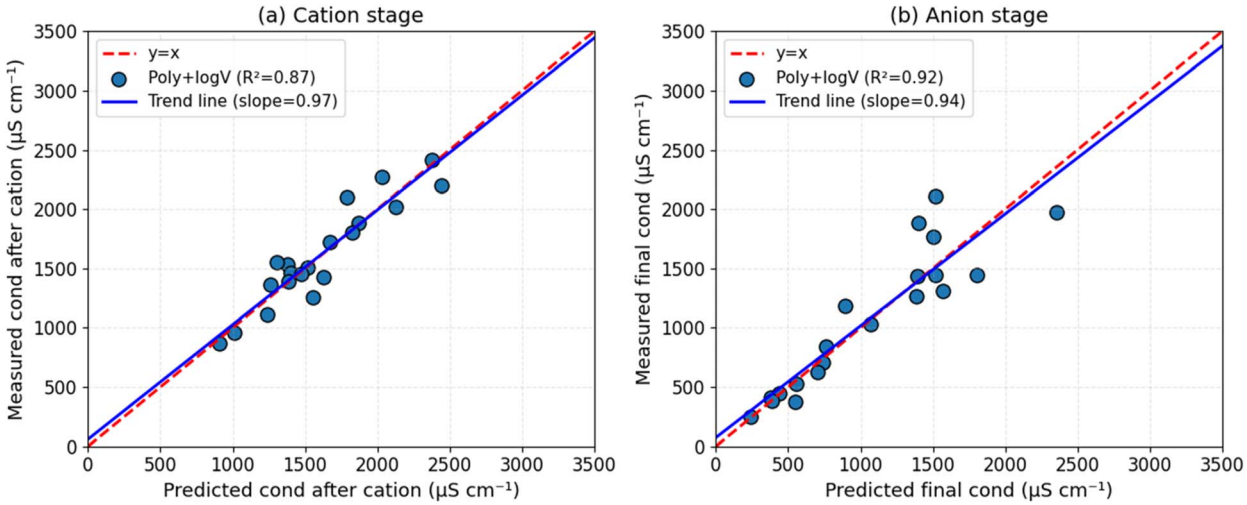

Fig. 4 Measured *versus* predicted conductivity after (a) cation exchange and (b) anion exchange using second-order polynomial regression models ($R^2 = 0.87$ and 0.92, respectively). The trendline slopes for the cation- and anion-exchange stages were 0.97 and 0.94. The dashed lines indicate the line of parity. Regression details are provided in the SI.

batch ion-exchange experiments. The experimental design spanned syrup volumes of 10–300 mL, contact times of 10–30 min per exchange stage, and inlet conductivities near 2.4 mS cm^{-1}. Resin dosages were normalized by syrup volume and expressed as cation (D_c) and anion (D_a) loadings (g resin per mL syrup). Details of the regression methodology and full dataset are provided in the SI (Section S1 and Table S1).

3.6.1. Cation-exchange regression. A second-order polynomial regression was used to relate the conductivity after cation exchange to the inlet conductivity, cation resin dosage, and contact time. The resulting model accurately captured the nonlinear behavior associated with ion-exchange saturation, achieving a coefficient of determination of $R^2 = 0.87$ (Fig. 4a). The curvature observed in the model response indicates diminishing conductivity reduction at higher resin loadings and longer contact times, consistent with diffusion- and capacity-limited cation exchange.

3.6.2. Anion-exchange regression. An analogous second-order model was developed for the anion-exchange stage using the conductivity exiting the cation step, anion resin dosage, and contact time as predictors. The anion-exchange model exhibited similarly strong predictive capability ($R^2 = 0.92$; Fig. 4b) and revealed pronounced nonlinear behavior at elevated resin dosages. This response reflects saturation effects and mass-transfer limitations typical of anion exchange in concentrated sugar syrups.

3.6.3. Bench-scale process optimization. Both regression models were used to identify operating conditions that achieve substantially reduced syrup conductivity, consistent with levels commonly targeted for downstream food and bioprocessing applications. The model identified an optimal operating region characterized by moderate cation-exchange resin dosages ($D_c \approx$ 0.04–0.17 g mL^{-1}), lower anion-exchange resin dosages ($D_a \approx$ 0.01–0.08 g mL^{-1}), and contact times of approximately 5–30 min per exchange stage. Under these conditions, the predicted syrup conductivity approached low-conductivity values ($\approx$250–300 µS cm^{-1}) while maintaining near-neutral pH. In contrast, lower resin dosages ($D_c < 0.07$ g mL^{-1} or $D_a < 0.02$ g mL^{-1}) generally resulted in incomplete deionization, with outlet conductivities frequently exceeding 500 µS cm^{-1}.

To assess the predictive capability of the polynomial regression model, a verification experiment was conducted using 300 mL of tagatose–galactose syrup with an initial conductivity of 2.3 mS cm^{-1}. This condition corresponds to the upper limit of the calibration range (10–300 mL) and was used to evaluate model performance at larger processing volumes. The optimized dosage ratios predicted by the model were scaled linearly with syrup volume, resulting in approximately 45 g of cation-exchange resin and a proportionally lower mass of anion-exchange resin, with 20 min contact time per stage. The cation resin was regenerated using 0.5 M HCl and the anion resin using 0.3 M NaOH, followed by rinsing until the rinse effluent conductivity fell below 200 µS cm^{-1}. Under these conditions, the syrup conductivity decreased from 2.3 mS cm^{-1} to 774 µS cm^{-1} after the cation-exchange step and to approximately 200 µS cm^{-1} after the anion-exchange step, following the reduction trends predicted by the model. This result demonstrates the reproducibility of the optimized ion-exchange strategy and confirms internal model consistency within the

Table 5 Model performance: correlation and overall significance

Response	Pearson *r*	Pearson *p*-value	ANOVA *F*	ANOVA *p*-value
Cation conductivity	0.93	<0.001	4.08	0.036
Anion conductivity	0.91	<0.001	7.15	0.007
pH	0.94	<0.001	4.26	0.032

bench-scale range studied (10–300 mL). This result does not constitute process scale-up in an engineering sense, but demonstrates that the empirical dosage relationships are reproducible across the volume range evaluated.

Predicted and measured values showed strong agreement across all responses (Table 5). Pearson correlation analysis indicated high correlations for the cation-exchange stage ($r = 0.93$, $p < 0.001$), anion-exchange stage ($r = 0.91$, $p < 0.001$), and pH ($r = 0.94$, $p < 0.001$). Analysis of variance confirmed that all regression models were statistically significant, with p-values of 0.036, 0.007, and 0.032 for the cation, anion, and pH models, respectively. The trendline slopes for the cation- and anion-exchange stages were 0.97 and 0.94, indicating that predicted and measured values are closely aligned, with only minimal deviation from perfect agreement.

3.7. Evaporation and final evaluation of concentrated tagatose–galactose syrups

Following ion-exchange deionization, the purified tagatose–galactose liquor (≈7–8 °Brix) was concentrated by vacuum evaporation to produce two final high-solids syrups at 65 and 75 °Brix. These syrups represent the final product streams of the process and were subjected to physicochemical, compositional, elemental, and microbiological evaluation. Because high-solids carbohydrate syrups exhibit elevated viscosity, reduced ion mobility, and non-ideal optical behavior, appropriate analytical handling was applied for several measurements to ensure accuracy and reproducibility.[27] The resulting data are summarized in Table 6 and discussed below.

3.7.1. Solids content and analytical handling of high-Brix syrups. Vacuum evaporation achieved the intended concentration endpoints with high reproducibility, yielding syrups at 65.0 ± 0.2 °Brix and 75.0 ± 0.2 °Brix (Table 6). Measurement of soluble solids by refractometry is well suited for high-sugar matrices and was therefore performed directly on the concentrated syrups. In contrast, electrochemical measurements such as electrical conductivity are known to be unreliable when performed directly on highly concentrated carbohydrate solutions, due to increased viscosity, suppression of ion mobility, and non-linear electrode response. For this reason, conductivity measurements were carried out on 10× diluted syrup samples prior to analysis (Table 6). The use of standardized dilution for conductivity determination is a common practice in the analysis of concentrated carbohydrate syrups, including refined glucose and fructose syrups, where dilution minimizes matrix effects while preserving relative ionic composition.[28,29]

3.7.2. Ionic quality after evaporation: conductivity, ash, and elemental purity. Electrical conductivity, measured on 10× diluted samples, increased from 376 ± 20 μS cm^{-1} at 65 °Brix to 455 ± 20 μS cm^{-1} at 75 °Brix (Table 6). These values represent method-defined, diluted measurements and are therefore used as comparative indicators of ionic removal rather than absolute conductivity values of the native concentrated syrups. The observed increase reflects concentration-dependent changes in ionic strength and equilibria following water removal rather than deterioration of deionization performance. Total ash content remained low following evaporation and showed no increasing trend with higher °Brix, decreasing slightly from 0.13 ± 0.02 wt% to 0.09 ± 0.02 wt% (Table 6). In addition, elemental analysis confirmed that Pb, Cd, As, and Hg were all below the limits of detection by ICP-OES.[30] Together, these results demonstrate that vacuum evaporation did not introduce

Table 6 Physicochemical, compositional, and microbiological properties of concentrated syrups[a]

	Unit	65 °Brix syrup	75 °Brix syrup	Method
Tagatose	wt% (dry basis)	53.5	56.2	HPLC-RI
Galactose (main impurity)	wt% (dry basis)	39.3	38.4	HPLC-RI
Minor sugars	wt% (dry basis)	7.2	5.4	HPLC-RI
Brix	°Brix	65.0 ± 0.2	75.0 ± 0.2	Digital refractometer
pH (25 °C)	—	7.30 ± 0.05	6.95 ± 0.05	pH meter
Water activity (a_w)	—	0.74 ± 0.01	0.70 ± 0.01	Water activity meter
Conductivity	μS cm^{-1}	376 ± 20	455 ± 20	Conductivity meter
Total ash	wt%	0.13 ± 0.02	0.09 ± 0.02	Gravimetric
Color (A_{420})	—	0.009 ± 0.001	0.011 ± 0.001	UV-vis
ICUMSA color	IU	90 ± 10	110 ± 10	Calculated from A_{420}
Pb	ppm	<LOD	<LOD	ICP-OES
Cd	ppm	<LOD	<LOD	ICP-OES
As	ppm	<LOD	<LOD	ICP-OES
Hg	ppm	<LOD	<LOD	ICP-OES
HMF	mg kg^{-1}	4.2 ± 0.5	8 ± 2	HPLC-UV
TAMC	CFU mL^{-1}	37.5	43	Plate count
Yeast & mold	CFU mL^{-1}	225	275	Plate count
Escherichia coli	—	N.D.	ND	Presence/absence
Salmonella spp.	—	N.D.	ND	Presence/absence
Staphylococcus aureus	—	N.D.	ND	Presence/absence

[a] Values are reported as mean ± standard deviation ($n = 2$) for each concentration level. N.D. indicates not detected, and LOD indicates the limit of detection. Sugar composition is reported on an organic dry basis excluding ash content; therefore, values sum to 100% of the organic fraction. Microbiological results are expressed as CFU mL^{-1} due to the liquid nature of the syrup samples.

inorganic contamination and that the effectiveness of upstream deionization was preserved during concentration, consistent with the behavior reported for refined carbohydrate syrups such as HFCS, where ion-exchange deashing followed by evaporation concentrates sugars without increasing inorganic impurities.[31,32]

3.7.3. Color development and thermal stability during concentration. Color development during evaporation was evaluated using A_{420} and ICUMSA color values (Table 6). Both parameters showed a gradual increase with increasing °Brix, with A_{420} rising from 0.009 ± 0.001 at 65 °Brix to 0.011 ± 0.001 at 75 °Brix and ICUMSA color increasing from 90 ± 10 to 110 ± 10 IU. This limited magnitude of color increase is consistent with mild thermal effects under vacuum conditions, where reduced boiling temperatures restrict extensive browning reactions such as caramelization and advanced Maillard chemistry.[33–35] Incremental color development with increasing solids content is well documented for refined carbohydrate syrups including glucose, fructose, and HFCS, and is generally attributed to concentration-dependent thermal effects rather than chemical degradation or impurity accumulation.[36] In industrial HFCS processing, similar modest increases in ICUMSA color are commonly observed during evaporation following ion-exchange purification, while maintaining low ash and metal contents.[36,37] The absence of concurrent increases in total ash or detectable metals (Pb, Cd, As, Hg) in Table 6 supports this interpretation, confirming that color development arose primarily from controlled thermal concentration rather than inorganic contamination or deterioration of deionization performance.

3.7.4. Formation of 5-hydroxymethylfurfural (HMF). Thermal degradation during evaporation was further assessed by quantifying HMF, a widely used indicator of heat-induced sugar degradation.[38–44] HMF concentrations remained low, below 5 mg kg^{-1} at 65 °Brix and increased slightly to 8 ± 2 mg kg^{-1} at 75 °Brix (Table 6). These values are consistent with evaporation under reduced pressure and limited thermal exposure and fall within ranges reported for refined carbohydrate syrups processed under controlled conditions.[25,45] The low HMF levels align with the modest color development observed and confirm that vacuum evaporation preserved sugar integrity despite the high final solids content.

3.7.5. Water activity and microbiological quality. Vacuum evaporation substantially reduced water activity, reaching 0.74 ± 0.01 at 65 °Brix and 0.70 ± 0.01 at 75 °Brix (Table 6). These water activity values fall within a range widely recognized to inhibit the growth of most spoilage microorganisms in sugar-rich systems, where reduction of water activity serves as the primary preservation mechanism for concentrated liquid sweeteners, including HFCS and other refined carbohydrate syrups.[46,47] Microbiological quality of the concentrated syrups, evaluated after short-term refrigerated storage, showed low total aerobic mesophilic counts (37.5–43 CFU mL^{-1}) and moderate yeast and mold counts (225–275 CFU mL^{-1}) for the 65 and 75 ° Brix samples, respectively (Table 6). No pathogenic microorganisms, including *Escherichia coli*, *Salmonella* spp., or *Staphylococcus aureus*, were detected in any sample. These results are consistent with reported microbiological profiles of concentrated tagatose-galactose syrups produced *via* ion-exchange and evaporation, including patented formulations exhibiting similarly low bacterial counts and absence of pathogens at comparable solids contents.[48] The observed yeast and mold levels are therefore attributed to storage-related effects rather than process-induced contamination, confirming satisfactory short-term microbiological stability of the syrup. Detailed microbiological enumeration data, including plate counts and dilution schemes, are reported in the SI (Table S2).

3.7.6. Sugar composition after evaporation. Sugar composition analysis confirmed the chemical stability of the syrup during vacuum concentration (Table 6). Tagatose remained the dominant carbohydrate at both concentration levels, accounting for 53.5 wt% (organic dry basis) at 65 °Brix and 56.2 wt% at 75 °Brix, while galactose persisted as the primary residual impurity. Minor sugars decreased slightly with increasing °Brix.

Although the present analysis focused on the major monosaccharides, prior patent disclosures describing tagatose–galactose syrups produced *via* alkaline epimerization and downstream purification indicate that such syrups may also contain minor non-sugar constituents. These include small amounts of oligosaccharides, glycerol, residual organic acids, and trace inorganic components originating from neutralization and ion-exchange steps, typically present at low weight fractions relative to the total carbohydrate content.[48] The stable monosaccharide composition observed here suggests that vacuum evaporation did not promote additional formation or transformation of these minor components, consistent with the compositional stability reported in the patent literature.

4. Conclusion

This study presents a process-level framework for producing tagatose–galactose syrup through the integration of CaO-promoted galactose isomerization, optimized neutralization, ion-exchange deionization, and controlled vacuum evaporation. Among the neutralization routes evaluated, CO_2 neutralization demonstrated clear advantages over sulfuric acid by generating a lower ionic load and enabling more effective downstream deionization, resulting in substantially reduced residual calcium, magnesium, and sulfur-containing species. Systematic screening of strong-acid cation and strong-base anion exchange resins identified an optimal resin combination capable of reducing syrup conductivity by approximately 90%, achieving conductivity levels as low as ~250 μS cm^{-1} under the tested conditions. Empirical regression models describing the effects of resin dosage and contact time provided reasonable agreement between predicted and measured values (R^2 = 0.87–0.92) and were successfully validated at larger syrup volumes, with trendline slopes of 0.97 and 0.94 for the cation- and anion-exchange stages, respectively, indicating excellent agreement between predicted and measured conductivity values. The developed model should be considered as an empirical framework for identifying trends and guiding preliminary process design, rather than a fully predictive tool for scale-up. Following

purification, vacuum evaporation to 65 and 75 °Brix produced stable, high-solids syrups with low ash content, acceptable ICUMSA color, minimal HMF formation, and preserved sugar composition, indicating that thermal concentration under reduced pressure did not compromise product quality. Microbiological evaluation after short-term refrigerated storage showed low aerobic counts, moderate yeast and mold levels, and absence of pathogens, consistent with the expected stability of concentrated carbohydrate syrups. Overall, this work demonstrates that CO_2-neutralized, ion-exchange-polished tagatose–galactose syrup approaches several quality benchmarks relevant to food applications at bench scale. Mass-based ion and sugar balances confirm that conductivity reductions reflect true ionic removal, and that both sugars are conserved quantitatively. The bench-scale operating guidelines and resin selection criteria established here provide a foundation for future column-scale process development and more comprehensive process validation.

Conflicts of interest

The authors declare no competing interests.

Data availability

The datasets generated during and/or analyzed during the current study are available from the authors on reasonable request.

Supplementary information (SI): the SI provides detailed descriptions of the regression modeling approach used for resin optimization, including model equations, fitting procedures, and the complete experimental dataset. In addition, raw microbiological data (plate counts, dilution factors, and calculated CFU values) are included to support the microbial analysis. SI figures illustrating syrup color differences between neutralization methods are also provided. See DOI: https://doi.org/10.1039/d6fb00038j.

Acknowledgements

This work is supported by the Agriculture and Food Research Initiative – Foundational and Applied Science Program, project award no. 2024-67018-42803, from the U.S. Department of Agriculture's National Institute of Food and Agriculture. Any opinions, findings, conclusions, or recommendations expressed in this publication are those of the author(s) and should not be construed to represent any official USDA or U.S. Government determination or policy.

References

1 M. Guerrero-Wyss, S. Durán Agüero and L. Angarita Dávila, *BioMed Res. Int.*, 2018, **2018**, 8718053.
2 A. de C. Ortiz, S. O. M. Fideles, C. H. B. Reis, B. T. Pagani, L. M. M. Bueno, M. B. M. Moscatel, R. L. Buchaim and D. V. Buchaim, *Nutrients*, 2024, **16**, 1943.
3 H. Zhang, X. Mao, Z. Lu, C. Gao, Z. Chen and J. Liu, *Fermentation*, 2025, **11**, 46.
4 D. Dai and Y. S. Jin, *Curr. Opin. Food Sci.*, 2024, **56**, 101137.
5 A. Muñoz-Labrador, R. Lebrón-Aguilar, J. E. Quintanilla-López, P. Galindo-Iranzo, S. M. Azcarate, S. Kolida, V. Kachrimanidou, V. García-Cañas, L. Methven, R. A. Rastall, F. J. Moreno and O. Hernández-Hernández, *J. Agric. Food Chem.*, 2022, **70**, 9048–9056.
6 Y. Lu, G. Wang, W. He, Y. Sun and M. Wang, *Bioresour. Technol.*, 2026, **445**, 134042.
7 P. Miao, Q. Wang, K. Ren, Z. Zhang, T. Xu, M. Xu, X. Zhang and Z. Rao, *Catalysts*, 2023, **13**, 1437.
8 J. Zhao, Z. Wang, Q. Jin, D. Feng and J. Lee, *J. Agric. Food Chem.*, 2023, **71**, 4228–4234.
9 J. R. Beadle, J. P. Saunders and T. J. Wajda, Process for manufacturing tagatose, *US Pat.*, US5002612, 1991.
10 J. R. Beadle, J. P. Saunders and T. J. Wajda, Process for manufacturing tagatose, *US Pat.*, US5078796, 1992.
11 A. R. Oroskar, Tagatose production from deproteinized whey and purification by continuous chromatography, *US Pat.*, US9150938B2, 2015.
12 N. Kim, J. Jeon, R. Chen and X. Su, *Chem. Eng. Res. Des.*, 2022, **178**, 267–288.
13 I. N. W. Khoiruddin and I. G. Wenten, *J. Food Eng.*, 2014, **133**, 40–45.
14 S. Babaei, N. Arabi, X. Shi, G. W. Huber, E. Camprubi and J. Zhao, *Ind. Eng. Chem. Res.*, 2025, **64**, 18656–18663.
15 T. Preechakun, S. Pongchaiphol, V. Champreda, N. Laosiripojana and M. Raita, *Biomass Bioenergy*, 2025, **197**, 107826.
16 X. F. Chen, H. L. Li, X. R. Ji, Z. J. Shen, H. J. Guo, S. M. Yao, M. K. Wang, L. Xiong and X. D. Chen, *Sep. Purif. Technol.*, 2023, **315**, 123661.
17 W. Chomchuen, L. Simasatitkul, W. Mens, S. Jantasee and C. Chaiya, *Results Eng.*, 2025, **25**, 103705.
18 P. I. Omwene, Z. B. O. Sarihan, A. Karagunduz and B. Keskinler, *Food Bioprod. Process.*, 2021, **129**, 1–9.
19 X. Wen, H. Lin, G. Liu, Y. Ning, Y. Ren, C. Li, C. Zhang, N. Dong, J. Lin, X. Song, G. Zhuang and J. Lin, *Food Microbiol.*, 2025, **131**, 104785.
20 X. Wen, H. Lin, G. Liu, Y. Ning, X. Xu, H. Hu, Y. Ren, C. Li, C. Zhang, N. Dong, X. Song, J. Lin and J. Lin, *Food Res. Int.*, 2025, **207**, 116109.
21 K. Hashimoto, K. Sakaguchi, R. Kono, S. Adachi and Y. Watanabe, *Food Bioprod. Process.*, 2025, **150**, 151–158.
22 ICUMSA, *New Numbers for GS2 White Sugar Methods*, https://www.icumsa.org/new-numbering-system/new-numbers-for-gs2-white-sugar-methods/.
23 İ. B. Can, Ö. Bıçak, S. Özçelik, M. Can and Z. Ekmekçi, *Minerals*, 2020, **10**, 1–17.
24 F. G. Helfferich, *Ion Exchange*, McGraw-Hill, New York, 1962.
25 J. S. White, *Am. J. Clin. Nutr.*, 2008, **88**, 1716S–1721S.
26 M. W. Kearsley and S. Z. Dziedzic, *Handbook of Starch Hydrolysis Products and Their Derivatives*, Springer, New York, 1995.
27 J. Małecki, I. Tomasevic and B. G. Sołowiej, *J. Food Qual.*, 2022, **2022**, 2317676.

28 B. Subbiah, A. L. Stembridge and K. R. Morison, Measurement and Calculation of the Electrical Conductivity of Model Honey Solutions, in *APCChE 2015 Congress Incorporating Chemeca*, 2015, Melbourne, Australia.
29 ICUMSA, *ICUMSA Method GS2-17: the Determination of Conductivity Ash in Refined Sugar Products and in Plantation White Sugar*, 2011.
30 ISO, *ISO 11885:2007: Water Quality — Determination of Selected Elements by Inductively Coupled Plasma Optical Emission Spectrometry (ICP-OES)*, 2007.
31 ISO, *ISO 24683:2022: High Fructose Syrup—Specifications and Test Methods*, 2022.
32 L. M. Hanover and J. S. White, *Am. J. Clin. Nutr.*, 1993, **58**, 724S–732S.
33 ICUMSA, *ICUMSA Method GS2-9: the Determination of Sugar Solution Colour at pH 7.0*, 2024.
34 J. Liu, P. Wan, C. Xie and D. W. Chen, *LWT–Food Sci. Technol.*, 2023, **182**, 114834.
35 K. Julai, P. Sridonpai, C. Ngampeerapong, K. Tongdonpo, U. Suttisansanee, W. Kriengsinyos, N. On-Nom and N. Tangsuphoom, *Foods*, 2023, **12**, 1268.
36 Purolite, Corn Sweetener Refining with Ion Exchange Resins, https://www.purolite.com/index/core-technologies/industry/food-and-beverage/sweetener-applications/corn-sweetener-refining-with-ion-exchange-resins.
37 Puritech, Food Processing: Fructose/Glucose, https://www.puritech.be/food-processing/fructose-glucose/.
38 M. Gupta, S. Kapoor, M. Bala, B. Vipin and C. Mahajan, *Food Technol. Biotechnol.*, 2025, **63**, 480–492.
39 M. C. Brinkman, A. A. Teferra, N. O. Kassem and N. O. F. Kassem, *Tob. Control*, 2019, **29**, S110–S116.
40 B. Fallico, E. Arena and M. Zappalà, *J. Food Sci.*, 2008, **73**, C625–C631.
41 S. Krainer, R. Brodschneider, J. Vollmann, K. Crailsheim and U. Riessberger-Gallé, *Ecotoxicology*, 2016, **25**, 320–328.
42 B. W. LeBlanc, G. Eggleston, D. Sammataro, C. Cornett, R. Dufault, T. Deeby and E. S. Cyr, *J. Agric. Food Chem.*, 2009, **57**, 7369–7376.
43 N. Arabi, S. Babaei, J. Qi, S. Arvelli and J. Zhao, *Biomass Futures*, 2026, **1**, 100009.
44 A. T. A. Asiz, *Physicochemical and Structural Optimization of Date (Phoenix Dactylifera L.) Syrup: Impact of Extraction Temperatures and Pectin Addition*, Master's thesis, United Arab Emirates University, 2025.
45 U. M. Shapla, M. Solayman, N. Alam, M. I. Khalil and S. H. Gan, *Chem. Cent. J.*, 2018, **12**, 35.
46 M. Starzak and M. Mathlouthi, *Zuckerindustrie*, 2002, **127**, 175–185.
47 M. Sramek, B. Woerz, H. Horn, J. Weiss and R. Kohlus, *J. Sci. Food Agric.*, 2017, **97**, 1178–1184.
48 I. Spa, Tagatose and galactose syrup, *US Pat.*, US12180553B2, Johns Hopkins University, 2024.